J|A|C|S
ARTICLES
Published on Web 10/20/2004

"Inverse-Electron-Demand" Ligand Substitution: Experimental and Computational Insights into Olefin Exchange at Palladium(0)

Brian V. Popp, Joseph L. Thorman, Christine M. Morales, Clark R. Landis,* and Shannon S. Stahl*

Contribution from the Department of Chemistry, University of Wisconsin—Madison, 1101 University Avenue, Madison, Wisconsin 53706

Received July 6, 2004; E-mail: landis@chem.wisc.edu; stahl@chem.wisc.edu

Abstract: The mechanism of olefin substitution at palladium(0) has been studied, and the results provide unique insights into the fundamental reactivity of electron-rich late transition metals. A systematic series of bathocuproine−palladium(0) complexes bearing *trans*-β-nitrostyrene ligands ($ns^X = X{-}C_6H_4CH{=}CHNO_2$; X = OCH_3, CH_3, H, Br, CF_3), (bc)Pd^0ns^X (**3**^{X}), was prepared and characterized, and olefin-substitution reactions of these complexes were found to proceed by an associative mechanism. In cross-reactions between (bc)Pd(ns^{CH_3}) and ns^X (X = OCH_3, H, Br, CF_3), more-electron-deficient olefins react more rapidly (relative rate: $ns^{CF_3} > ns^{Br} > ns^H > ns^{OCH_3}$). Density functional theory calculations of model alkene-substitution reactions at a diimine−palladium(0) center reveal that the palladium center reacts as a nucleophile via attack of a metal-based lone pair on the empty π^* orbital of the incoming olefin. This orbital picture contrasts that of traditional ligand-substitution reactions, in which the incoming ligand donates electron density into an acceptor orbital on the metal. On the basis of these results, olefin substitution at palladium(0) is classified as an "inverse-electron-demand" ligand-substitution reaction.

Introduction

Electron-rich late transition metals play a prominent role in catalytic reactivity. Important examples include palladium(0)-catalyzed cross-coupling reactions (eqs 1−3),[1] nickel(0)-catalyzed reductive coupling of unsaturated substrates, including carbon dioxide (eqs 4 and 5),[2] and copper(I)-mediated conjugate additions reactions (eq 6).[3,4] The transition metals in these reactions possess fully occupied d-orbitals (i.e., d^{10}), and their electron-rich, nucleophilic character is manifested by their reactivity with electron-deficient, electrophilic substrates.

Our laboratory has been interested recently in palladium-catalyzed oxidation reactions.[5] These reactions are usually described from the perspective of the palladium(II)-mediated process (step I, Scheme 1), but efficient reoxidation of the electron-rich palladium(0) intermediate (step II, Scheme 1) is

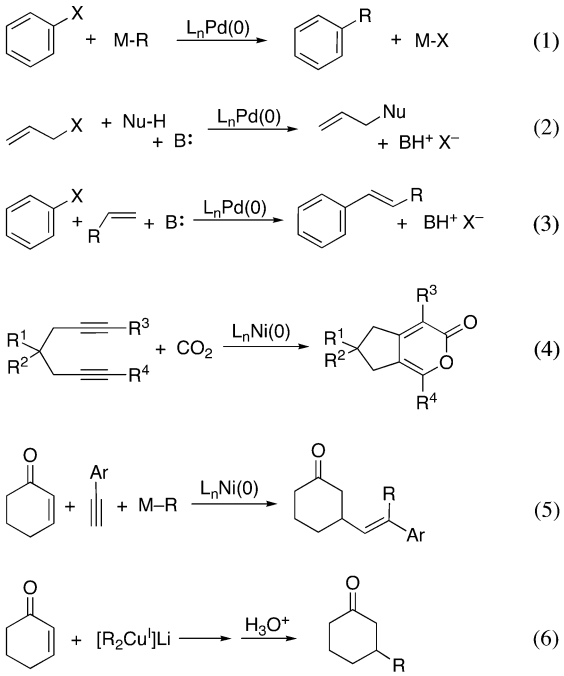

critical to the success of the catalytic reaction. In this context, we have been investigating the fundamental reactivity of palladium(0), particularly with respect to its reaction with molecular oxygen.[6] The diimine-coordinated palladium(0) complex, (bc)Pd(dba) (**1**) (bc = bathocuproine or 2,9-dimethyl-4,7-diphenyl-1,10-phenanthroline; dba = dibenzylideneacetone), undergoes oxidative addition of molecular oxygen to yield a

(1) (a) Diederich, F., Stang, P. J., Eds. *Metal-Catalyzed Cross-Coupling Reactions*; Wiley-VCH: New York, 1998. (b) Trost, B. M.; Van Vranken, D. L. *Chem. Rev.* **1996**, *96*, 395−422. (c) Beletskaya, I. P.; Cheprakov, A. V. *Chem. Rev.* **2000**, *100*, 3009−3066. (d) Muci, A. R.; Buchwald, S. L. *Top. Curr. Chem.* **2002**, *219*, 131−209. (e) Hartwig, J. F. *Angew. Chem., Int. Ed.* **1998**, *37*, 2046−2067.

(2) (a) Montgomery, J. *Angew. Chem., Int. Ed.* **2004**, *43*, 3890−3908. (b) Takimoto, M.; Nakamura, Y.; Kimura, K.; Mori, M. *J. Am. Chem. Soc.* **2004**, *126*, 5956−5957. (c) Louie, J.; Gibby, J. E.; Farnworth, M. V.; Tekavec, T. N. *J. Am. Chem. Soc.* **2002**, *124*, 15188−15189. (d) Takimoto, M.; Mori, M. *J. Am. Chem. Soc.* **2002**, *124*, 10008−10009. (e) Takimoto, M.; Mori, M. *J. Am. Chem. Soc.* **2001**, *123*, 2895−2896.

(3) (a) Krause, N., Ed. *Modern Organocopper Chemistry*; Wiley-VCH: New York, 2002. (b) Nakamura, E.; Mori, S. *Angew. Chem., Int. Ed.* **2000**, *39*, 3750−3771.

(4) A number of copper-catalyzed conjugate additions of organozinc reagents to α,β-unsaturated carbonyl compounds employ a copper(II) source (see ref 3a); in situ reduction of the metal to copper(I) probably occurs under the catalytic conditions.

(5) Stahl, S. S. *Angew. Chem., Int. Ed.* **2004**, *43*, 3400−3420.

10.1021/ja0459734 CCC: $27.50

Scheme 1. Simplified Catalytic Cycle for Palladium-Catalyzed Oxidation Reactions

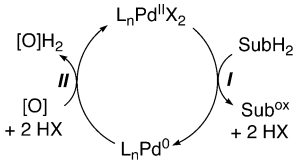

peroxopalladium(II) species, **2** (eq 7). This reaction proceeds by an associative pathway that resembles the mechanism of ligand substitution at palladium(0).[7] To provide a direct comparison between oxygenation and ligand-substitution reactions, we have investigated olefin-substitution reactions at palladium(0) complexes bearing identical ancillary ligation (eq 8).

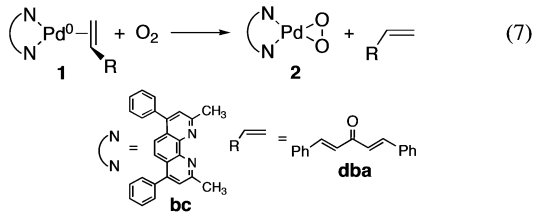

(7)

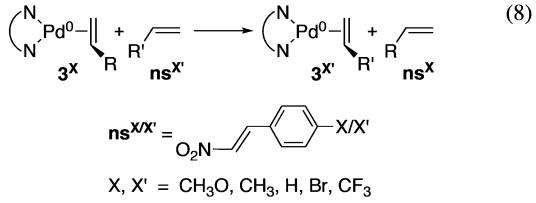

(8)

Ligand-substitution reactions are among the most fundamental transformations at transition-metal centers and have been the subject of extensive study.[8] Both associative and dissociative mechanistic pathways have been characterized, together with a continuum of intermediate mechanisms that exhibit differing degrees of associative or dissociative character. Dissociative mechanisms generally arise for coordinatively saturated, 18-electron complexes that require ligand dissociation to vacate an orbital at the metal center for attack by the incoming ligand. In contrast, associative ligand-substitution reactions generally arise for coordinatively unsaturated (<18-electron) complexes, which possess empty or partially filled metal-based orbitals in the ground state. Despite these distinctions, a unifying mechanistic principle among all of these reactions is the description of the incoming ligand as the *donor* and the metal as the *acceptor* of electron density. The assignment of nucleophilicity parameters, *n*, for a wide variety of ligands[9] reinforces this mechanistic picture. From a simplified molecular orbital perspective, ligand-substitution reactions are initiated by the interaction between the highest occupied molecular orbital (HOMO) on the ligand and the lowest unoccupied molecular orbital (LUMO) on the metal (Figure 1). The reaction rate can be enhanced by raising the ligand LUMO energy (increasing its nucleophilicity) or by lowering the metal HOMO energy (increasing its electrophilicity).

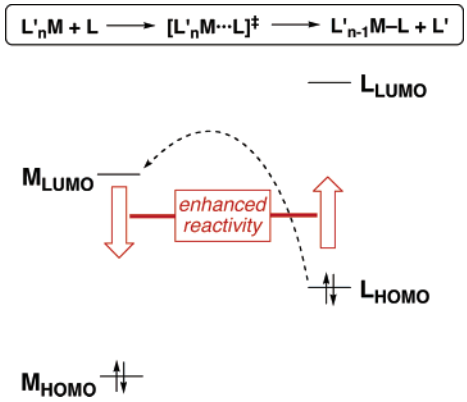

Figure 1. Simplified molecular-orbital analysis of an associative ligand-substitution reaction at a transition-metal center. The primary orbital overlap occurs between a ligand-based HOMO and a metal-based LUMO, and improved overlap will lead to higher reaction rates.

The present study describes olefin-substitution reactions at palladium(0) that violate these reactivity patterns.[10] Experimental studies reveal that the electron-rich palladium(0) center reacts as a donor (nucleophile) and the incoming olefin as an acceptor (or electrophile) in the reaction, and density functional theory (DFT) calculations outline the molecular orbital interactions that underlie this behavior. Such reactivity, designated "inverse-electron-demand" ligand substitution, probably occurs in numerous other electron-rich transition-metal systems, and therefore, insights from the present studies provide an important framework for rationalizing and predicting the reactivity of these metal centers in catalytic chemistry.

Results and Discussion

Olefin Self-Exchange Reactions between (bc)Pd(dba) and dba. Our initial studies of olefin substitution at bathocuproine-coordinated palladium(0) involved dibenzylideneacetone (dba) self-exchange reactions with (bc)Pd(dba), **1**. X-ray crystallographic characterization of **1** reveals that only one of the two olefins in the dba ligand coordinates to the palladium center.[6a] The ^{1}H NMR spectrum of **1** in CD_2Cl_2 reveals that this coordination mode is retained in solution, and the complex is not fluxional on the NMR time scale. When free dba is added to a solution of **1**, however, the ^{1}H NMR spectrum reveals fluxional behavior at room temperature. In the presence of 8 equiv of dba, resonances of the coordinated olefin protons (4.16 and 4.49 ppm) and the unsymmetrical methyl groups of the bathocuproine ligand (2.97 and 3.21 ppm) coalesce at 27.5(1.5) and 17.5(1.5) °C, respectively (Figure 2). Detailed kinetics of this exchange reaction were attempted by measuring the ^{1}H NMR line width at different concentrations of exogenous dba, but these studies were hindered by the presence of ~10% of another palladium−

(6) (a) Stahl, S. S.; Thorman, J. L.; Nelson, R. C.; Kozee, M. A. *J. Am. Chem. Soc.* **2001**, *123*, 7188−7189. (b) Konnick, M. M.; Guzei, I. A.; Stahl, S. S. *J. Am. Chem. Soc.* **2004**, *126*, 10212−10213.

(7) (a) Ozawa, F.; Ito, T.; Nakamura, Y.; Yamamoto, A. *J. Organomet. Chem.* **1979**, *168*, 375−391. (b) van Asselt, R.; Elsevier, C. J.; Smeets, W. J. J.; Spek, A. L. *Inorg. Chem.* **1994**, *33*, 1521−1531. (c) Canovese, L.; Visentin, F.; Uguagliati, P.; Crociani, B. *J. Chem. Soc., Dalton Trans.* **1996**, 1921−1926. (d) Canovese, L.; Visentin, F.; Chessa, G.; Uguagliati, P.; Dolmella, A. *J. Organomet. Chem.* **2000**, *601*, 1−15.

(8) (a) Langford, C. H.; Gray, H. B. *Ligand Substitution Processes*; W. A. Benjamin: New York, 1966. (b) Collman, J. P.; Hegedus, L. S.; Norton, J. R.; Finke, R. G. *Principles and Applications of Organotransition Metal Chemistry*, 2nd ed.; University Science Books: Mill Valley, CA, 1987; pp 235−278. (c) Crabtree, R. H. *The Organometallic Chemistry of the Transition Metals*, 3rd ed.; Wiley: New York, 2001; pp 80−114.

(9) This classification has been extensively applied in ligand-substitution reactions of square-planar platinum(II) complexes: (a) Edwards, J. O.; Pearson, R. G. *J. Am. Chem. Soc.* **1962**, *84*, 16−24. (b) Belluco, U.; Cattalini, L.; Basolo, F.; Pearson, R. G.; Turco, A. *J. Am. Chem. Soc.* **1965**, *87*, 241−246. (c) Pearson, R. G.; Sobel, H.; Songstad, J. *J. Am. Chem. Soc.* **1968**, *90*, 319−326. (d) Becker, M.; Elias, H. *Inorg. Chim. Acta* **1986**, *116*, 47−62.

(10) A preliminary account of the experimental aspects of this work was recently reported: Stahl, S. S.; Thorman, J. L.; de Silva, N.; Guzei, I. A.; Clark, R. W. *J. Am. Chem. Soc.* **2003**, *125*, 12−13.

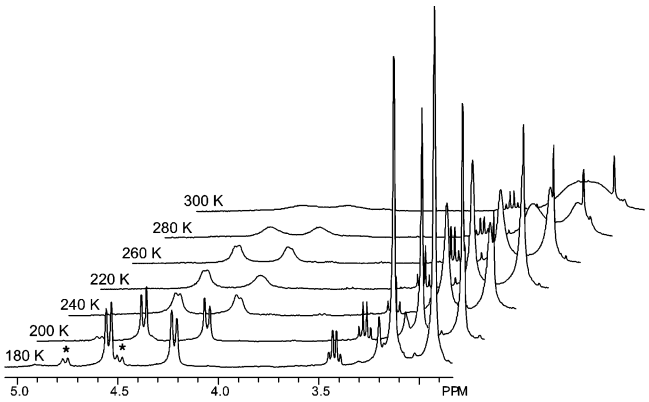

Figure 2. Temperature-dependent spectra of the dba self-exchange reaction with (bc)Pd(dba). Reaction conditions: [Pd] = 20 mM, [dba] = 160 mM, CD_2Cl_2. The resonances identified by an asterisk in the 180 K spectrum correspond to an impurity and/or isomer of **1** that participates in the fluxional process.

dba complex that participates in the fluxional process (see 180 K spectrum, Figure 2).[11,12] Despite this complication, the fluxional behavior in the presence of excess olefin provides qualitative support for an associative olefin-exchange process at the bathocuproine−palladium(0) center. To obtain more detailed mechanistic insights into olefin exhange, we shifted our attention to bathocuproine−palladium(0) complexes bearing β-nitrostyrene ligands (ns^X).

Synthesis and Characterization of (bc)Pd(ns^X) Derivatives. A series of (bc)Pd(ns^X) complexes (ns^X = X−C_6H_4CH═$CHNO_2$; X = OCH_3, CH_3, H, Br, and CF_3) were synthesized by addition of a slight excess (1.2 equiv) of the ns^X derivative to **1**, and the products, $\mathbf{3^X}$, were generally obtained in >60% yields (eq 9). Three of these adducts (X = H, CH_3, and Br)

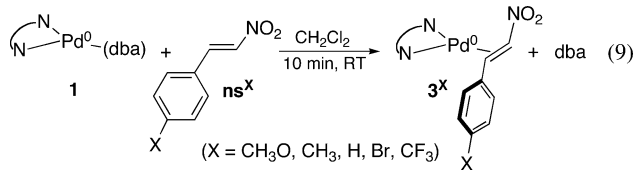

(9)

were characterized by single-crystal X-ray diffraction analysis,[13] and the structures exhibit a trigonal coordination environment that has been observed in other L_2Pd^0(olefin) complexes.[7,14] The carbon atoms of the coordinated olefin are nearly coplanar with the palladium and nitrogen atoms. The C−C bond lengths of the coordinated olefins, 1.427−1.437 Å, are significantly longer than those of the free olefins, 1.299−1.341 Å.[15] This feature is consistent with substantial back-bonding from palladium into the olefin π^* orbitals and highlights the significance of the pseudo-square-planar metallacyclopropane resonance structure for these complexes (eq 10).[16]

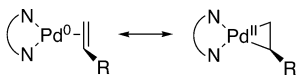

(10)

(11) Reid, S. M.; Mague, J. T.; Fink, M. J. *J. Organomet. Chem.* **2000**, *616*, 10−18.
(12) The identity of this complex is not known, but it possibly arises from an isomer of dba or the palladium−dba adduct. For example, s-cis/s-trans isomerization of the dba ligand has been proposed to account for fluxional behavior in palladium−dba complexes bearing chelating diphosphine ligands. See ref 11.
(13) For crystallographic data, see Supporting Information of ref 10.

Equilibrium Studies of Olefin Exchange. The palladium(0)−olefin complexes, $\mathbf{3^X}$, undergo rapid equilibrium exchange with free β-nitrostyrene derivatives in dichloromethane (eq 11).

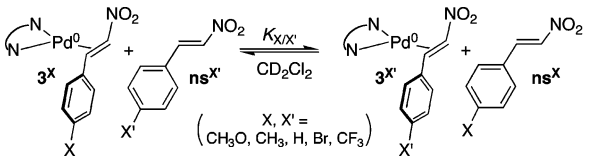

(11)

Equilibrium constants were obtained for several olefin partners at various temperatures (203−237 K) by ^{1}H NMR spectroscopy, and thermodynamic parameters were obtained by van't Hoff analysis of the data (Table 1).

Table 1. Equilibrium Constants and Thermodynamic Parameters for Equilibrium Olefin-Exchange Reactions (Eq 11)[a]

entry	X	X′	$K_{X/X'}$ (−70 °C)	$\Delta H°$ (kcal/mol)	$\Delta S°$ (eu)
1	Br	CF_3	13.5	−0.9	0.7
2	H	Br	7.0	−0.7	0.7
3	CH_3	H	4.6	−0.7	−0.4
4	OCH_3	H	23.7	−1.7	−2.2
5	OCH_3	CH_3	5.56	−0.8	−0.5

[a] The temperature-dependent equilibria in CD_2Cl_2 (eq 11) were monitored by ^{1}H NMR spectroscopy under an inert atmosphere (N_2).

From the individual equilibrium constants, relative binding constants were determined for the entire series. A Hammett plot reveals a linear correlation of these constants with the σ parameter of the para substituents (Figure 3). This result reflects a strong thermodynamic bias favoring coordination of more electron-deficient olefins to the (bc)Pd(0) fragment.[17]

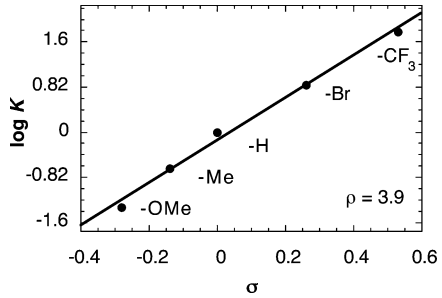

Figure 3. Hammett plot of the relative equilibrium constants for olefin coordination to the (bc)Pd(0) fragment at −70 °C in CD_2Cl_2.

Kinetic Studies of Olefin Exchange. The self-exchange reaction of dba at the (bc)Pd(0) center provided qualitative support for an associative substitution pathway (see above), but more detailed study was possible with the (bc)Pd(ns^X) complexes. The self-exchange reactions of four different nitrostyrene derivatives, ns^{OCH_3}, ns^{CH_3}, ns^{Br}, and ns^{CF_3}, with their corresponding (bc)Pd(ns^X) adducts were investigated by dynamic NMR

(14) (a) Ittel, S. D.; Ibers, J. A. *Adv. Organomet. Chem.* **1976**, *14*, 33−61. (b) Kluwer, A. M.; Elsevier, C. J.; Bühl, M.; Lutz, M.; Spek, A. L. *Angew. Chem., Int. Ed.* **2003**, *42*, 3501−3504.
(15) (a) Desiraju, G. R.; Pedireddi, V. R. *J. Chem. Soc., Chem. Commun.* **1989**, 1112−1113. (b) Pedireddi, V. R.; Sarma, J. A. R. P.; Desiraju, G. R. *J. Chem. Soc., Perkin Trans.* **1992**, *2*, 311−320.
(16) (a) Dewar, M. J. S. *Bull. Soc. Chim. Fr.* **1951**, *18*, C71−C79. (b) Chatt, J.; Duncanson, L. A. *J. Chem. Soc.* **1953**, 2939−2947.
(17) Previous thermodynamic studies of olefin binding to d^{10} transition-metal complexes have revealed similar behavior. See, for example: (a) Otsuka, S.; Yoshida, T.; Tatsuno, Y. *J. Am. Chem. Soc.* **1971**, *93*, 6462−6469. (b) Tolman, C. A. *J. Am. Chem. Soc.* **1974**, *96*, 2780−2789. (c) Ittel, S. D. *Inorg. Chem.* **1977**, *16*, 2589−2597.

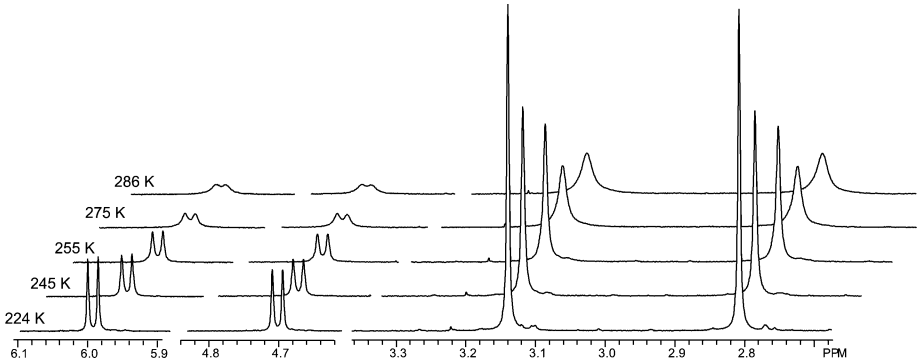

Figure 4. Temperature-dependent ^{1}H NMR spectra of ns^{CF_3} self-exchange reaction with (bc)Pd(ns^{CF_3}). Line-broadening of resonances in the coordinated alkene and bathocuproine−methyl regions of the spectra reflects the rapid alkene exchange reaction. Reaction conditions: [Pd] = 10 mM, [ns^{CF_3}] = 60 mM, CD_2Cl_2.

Table 2. Activation Parameters for Degenerate Olefin Exchange between (bc)Pd(ns^X) and ns^X [a]

entry	olefin	temp range (K)	k ($M^{-1}s^{-1}$), 25 °C	$\Delta H^{\ddagger}$ (kcal/mol)[b]	$\Delta S^{\ddagger}$ (eu)[b]
1	ns^{CF_3}	224−286	749	7.3	−24
2	ns^{Br}	253−284	492	8.8	−30
3	ns^{CH_3}	264−295	284	7.2	−24
4	ns^{OCH_3}	254−294	257	8.2	−27

[a] The temperature-dependent line broadening associated with olefin exchange was monitored by ^{1}H NMR spectroscopy under an inert N_2 atmosphere. [b] The errors associated with the activation parameters are $\Delta H^{\ddagger}$, ±1.0 kcal/mol, and $\Delta S^{\ddagger}$, ±3 eu.

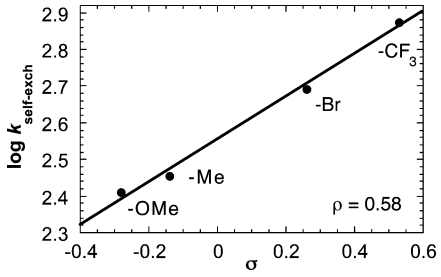

Figure 5. Hammett plot reflecting electronic effects on the olefin self-exchange rates for the different (bc)Pd(ns^X)/ns^X (X = OCH_3, CH_3, Br, CF_3) partners.

spectroscopic methods. Rapid exchange between free and coordinated olefin results in line-broadening of the resonances above ∼ −60 °C, and the line widths of the coordinated olefin resonances were used to determine the exchange rates at different temperatures (Figure 4).[18] Eyring plots of the temperature-dependent exchange rates (Figure S3, Supporting Information) enabled the determination of activation parameters for these reactions. Modest enthalpies of activation, 7.2−8.8 kcal/mol, and large negative entropies of activation, −24 to −30 eu, were obtained (Table 2). The self-exchange rates exhibit only a small dependence on substrate electronics. The shallow positive slope of the Hammett plot ($\rho = 0.58$, Figure 5) indicates that electron-deficient olefins exchange slightly more rapidly.

The self-exchange reaction of ns^{CF_3} with (bc)Pd(ns^{CF_3}) was also investigated at different olefin concentrations (Figure 6). The pseudo-first-order rate constants exhibit a linear dependence on [ns^{CF_3}], and the fit intersects the origin (Figure 7).

Cross-reactions between (bc)Pd(ns^{CH_3}) ($\mathbf{3}^{CH_3}$) and other β-nitrostyrene derivatives, ns^X, were studied by UV−visible spectroscopy. The free olefins have negligible absorption above 410 nm, and extinction coefficients for the different palladium complexes exhibit sufficient differences in the visible region to obtain reliable kinetics data. The reaction between $\mathbf{3}^{CH_3}$ and ns^{OCH_3} was studied in most detail because it proceeds at convenient rates under pseudo-first-order conditions. Addition of excess of ns^{OCH_3} (≥10 equiv) to $\mathbf{3}^{CH_3}$ in CH_2Cl_2 at room temperature promotes formation of $\mathbf{3}^{OCH_3}$ in >96% yield. The kinetic time-course of this reaction exhibits pseudo-first-order behavior (Figure 8A), and the rate constants, k_{obs}, exhibit a linear dependence on [ns^{OCH_3}] (Figure 8B).

This ligand-substitution reaction was also investigated in toluene, which has a substantially lower dielectric constant relative to that of dichloromethane ($\epsilon = 2.38$ vs 8.93, respectively), to assess the effect of solvent polarity on the reaction. Equilibrium constants, K_{CH_3/OCH_3} (eq 11), determined by ^{1}H NMR spectroscopy, are only slightly different in the two solvents at 300K: $K_{CH_3/OCH_3} = 0.40 \pm 0.05$ (CD_2Cl_2) and 0.25 ± 0.05 (toluene-d_8). Rates of the reaction between $\mathbf{3}^{CH_3}$ and ns^{OCH_3} were measured by UV−visible spectroscopy in solvent mixtures ranging from 93:7 toluene:CH_2Cl_2 to 100% CH_2Cl_2.[19] The reaction rate is first-order in [ns^{OCH_3}] throughout the entire solvent range (Figures 8B and S4A,B), and in all cases, plots of k_{obs} versus [ns^{OCH_3}] intersect the origin. The reaction rate for the formation of $\mathbf{3}^{OCH_3}$ is higher in toluene than in dichloromethane (Figure 9). The logarithmic relationship between k_{for} and ϵ^{-1} (inset, Figure 9) is consistent with theoretical predictions for reactions between neutral, dipolar molecules in solvents of different polarity.[20,21] This analysis predicts that the slope of the plot of ln(k) versus ϵ^{-1} will be positive if the dipole moment of the reactants is greater than that of the transition state. Computational studies (see below) support this prediction.

The reactions of $\mathbf{3}^{CH_3}$ with ns^H, ns^{Br}, and ns^{CF_3} (eq 12) were too rapid to monitor under pseudo-first-order conditions, but suitable rates were attained at lower olefin concentrations (1−2 equiv relative to $\mathbf{3}^{CH_3}$), conditions under which an equilibrium mixture of the two palladium−olefin complexes is formed.

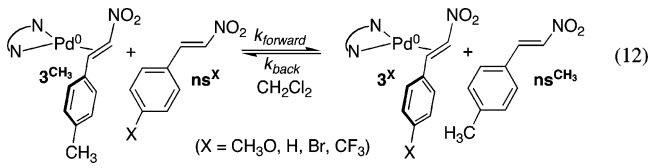

(12)

(18) Jackman, L. M., Cotton, F. A., Eds. *Dynamic Nuclear Magnetic Resonance Spectroscopy*; Academic Press: New York, 1975.

(19) Insufficient absorbance changes were observed in 100% toluene to obtain reliable kinetics.

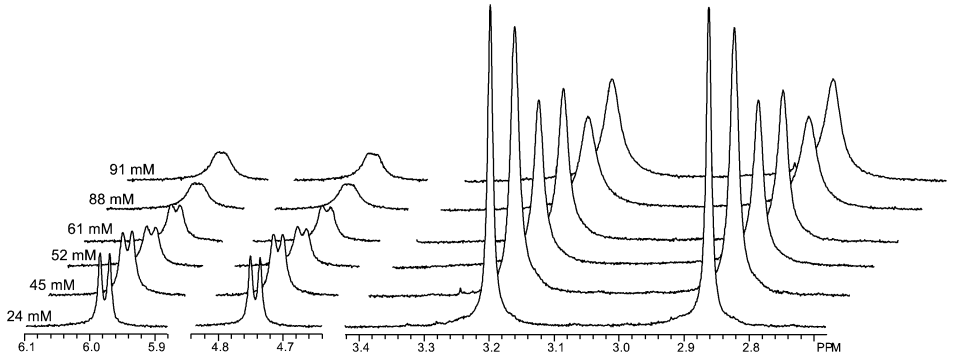

Figure 6. ^{1}H NMR spectra of ns^{CF_3} self-exchange reactions with (bc)Pd(ns^{CF_3}) in the presence of different concentrations of ns^{CF_3}. Reaction conditions: [Pd] = 10 mM, [ns^{CF_3}] = 24−91 mM, CD_2Cl_2, 286 K.

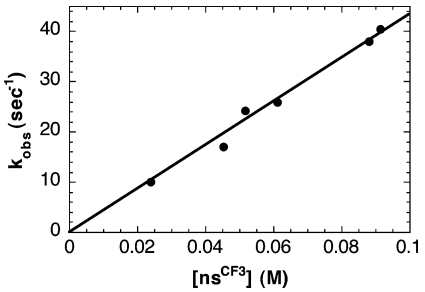

Figure 7. Olefin concentration dependence of the intermolecular exchange rate between (bc)Pd(ns^{CF_3}) and ns^{CF_3} based on ^{1}H NMR line-broadening kinetics. Reaction conditions: [Pd] = 10 mM, [ns^{CF_3}] = 24−91 mM, CD_2Cl_2, 286 K.

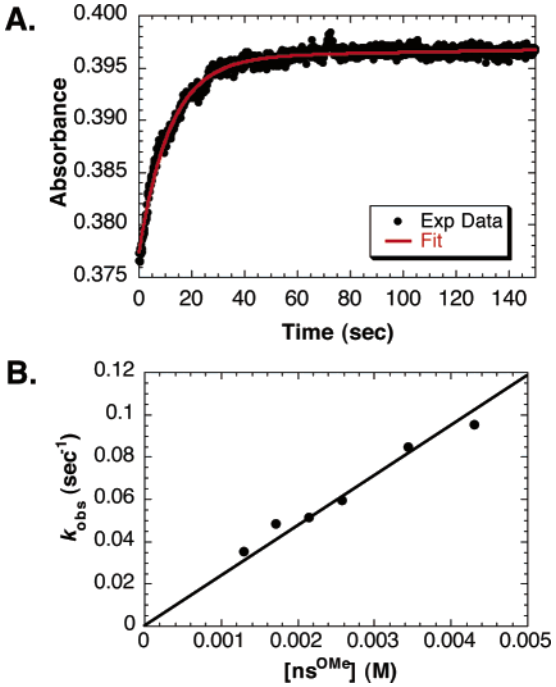

Figure 8. (A) Representative absorbance data (445 nm) and pseudo-first-order fit for the substitution of ns^{CH_3} by ns^{OCH_3} at (bc)Pd(0). (B) Pseudo-first-order olefin-concentration dependence for the associative ligand substitution of ns^{CH_3} by ns^{OCH_3}. Reaction conditions: [Pd] = 110 μM, [ns^{OMe}] =1.3−4.3 mM, 3.0 mL CH_2Cl_2, 298 K.

Kinetics of the approach to equilibrium were monitored by UV−visible spectroscopy. The time courses for each reaction were fit using numerical simulation methods (fourth-order Runge−Kutta) based on an approach-to-equilibrium kinetics model with second-order kinetics in both directions. The forward rate

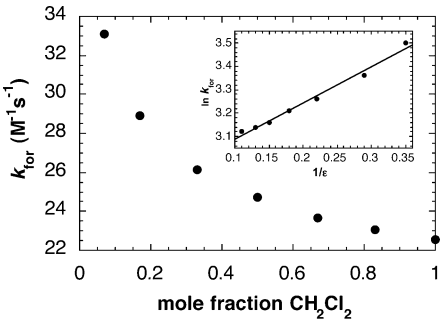

Figure 9. Solvent dependence on the forward rate constant for the substitution of ns^{OCH_3} for ns^{CH_3} in (bc)Pd(ns^{CH_3}), determined in mixtures of dichloromethane and toluene. Reaction conditions: [Pd] = 120 μM, [ns^{OCH_3}] = 2.0 mM, solvent toluene/CH_2Cl_2 = 93/7−0/100, 298 K.

constants derived from these fits reveal a systematic increase in the reaction rate with increasing electron-withdrawing character of the β-nitrostyrene substituent. A Hammett plot of the relative rate constants is linear, with a positive slope of 2.2 (Figure 10).

The electronic effects on these reactions are very unusual because ligand-substitution rates generally track with the electron-donating ability or nucleophilicity of the incoming ligand (see Introduction). To gain further insights into these observations, including electronic structure contributions to the reaction mechanism, the reactions have been investigated by density functional theory (DFT).

Computational Model Systems. For the purpose of computational studies, the bathocuproine and β-nitrostyrene ligands were simplified to the parent α-diimine ligand (di) and ethylene or nitroethylene (Chart 1). DFT calculations were conducted

(20) Reichardt, C. *Solvents and Solvent Effects in Organic Chemistry*, 3rd ed.; Wiley-VCH: New York, 2003.

(21) The inset plot in Figure 9 is based on the analysis reported by Kirkwood et al., who proposed the following relationship between the rate constant of a reaction in a solvent (k), the rate constant in a condensed medium with $\epsilon = 1$ (k_0), and the dipole moments of the reactants (μ_A, μ_B) and transition state ($\mu_\ddagger$). The terms r_A, r_B, and $r_\ddagger$ define the radius of the reactants and transition state, and ϵ_r is the dielectric constant of the solvent in question.

$$\ln k = \ln k_0 + \frac{1}{4\pi\epsilon_0}\frac{3N_A}{8RT}\left(\frac{2}{\epsilon_r} - 1\right)\left(\frac{\mu_A^2}{r_A^3} + \frac{\mu_B^2}{r_B^3} - \frac{\mu_\ddagger^2}{r_\ddagger^3}\right)$$

$$\text{slope} = \frac{1}{4\pi\epsilon_0}\frac{3N_A}{8RT}\left(\frac{\mu_A^2}{r_A^3} + \frac{\mu_B^2}{r_B^3} - \frac{\mu_\ddagger^2}{r_\ddagger^3}\right)$$

See ref 20 and the following primary references: (a) Kirkwood, J. G. *J. Chem. Phys.* **1934**, *2*, 351−361. (b) Kirkwood, J. G.; Westheimer, F. H. *J. Chem. Phys.* **1938**, *6*, 506−512. (c) Laidler, K. J.; Landskroener, P. A. *Trans. Faraday Soc.* **1956**, *52*, 200−210.

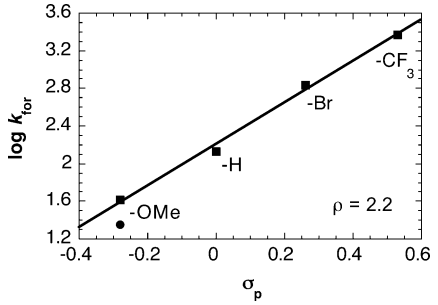

Figure 10. Hammett plot reflecting electronic effects on ligand substitution of ns^{CH_3} from (bc)Pd(ns^{CH_3}) by para-substituted nitrostyrene derivatives. Filled squares represent data obtained by fitting approach-to-equilibrium kinetics by numerical simulation methods. The filled circle reflects the rate obtained under pseudo-first-order conditions.

Chart 1. Experimental and Computational Ligands

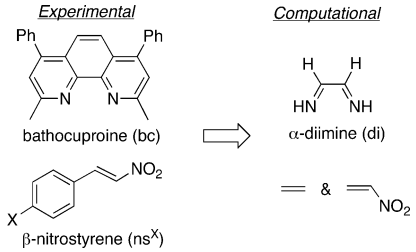

on the ground-state structures of the two palladium(0)−olefin complexes, (di)Pd(C_2H_4) (**4**) and (di)Pd($C_2H_3NO_2$) (**5**), and the reaction coordinate for the self-exchange reactions, **4** + C_2H_4 and **5** + $C_2H_3NO_2$. Initial DFT geometry optimizations employed the B3LYP functional and a standard double-ζ basis set with a relativistic effective core potential, LANL2DZ, to establish the structure and energy of both palladium complexes and the olefins. A higher-level basis set, Stuttgart RSC 1997 ECP, which incorporates a triple-ζ basis set with diffuse and polarization functions added to C, N, and H, was also utilized for the (di)Pd(C_2H_4)/C_2H_4 system. Use of the larger basis set resulted in minor changes to the optimized energies and geometries (Tables S5 and S6), but it did not alter the key conclusions outlined below.

Computational Structures of Ground States, Intermediates, and Transition States in Olefin Self-Exchange Reactions. Structural parameters of the computed structures, **4** and **5** (Figure 11), compare favorably with those of the (bc)Pd(ns^X) complexes obtained from X-ray crystallography (Table S3). Perhaps the most distinctive features are the elongated C−C bond of the coordinated olefin, for which very similar experimental and computational bond lengths were obtained: 1.427(14), 1.43, and 1.44 Å for $\mathbf{3}^H$ (X-ray), **4** (DFT), and **5** (DFT), respectively.[22]

Associative ligand-substitution reactions can take place via a stepwise or concerted mechanism, and these pathways are distinguished by the presence or absence of a (meta-)stable intermediate along the reaction coordinate. No intermediate is detected experimentally, but computational optimization of (di)-

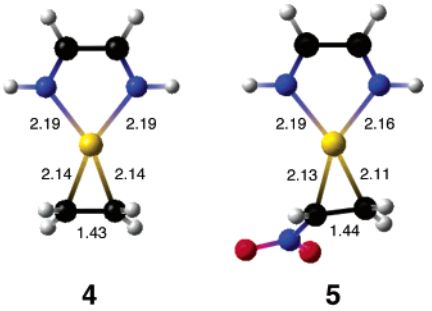

Figure 11. Ball-and-stick models of the minimized ground-state DFT structures obtained for (di)Pd(C_2H_4) (**4**) and (di)Pd($C_2H_3NO_2$) (**5**) in dichloromethane. Numerical values identify the calculated bond lengths (Å).

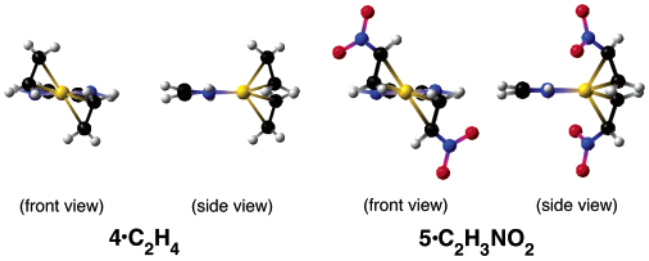

Figure 12. Ball-and-stick models of the minimized structures of diolefin adducts, (di)Pd(C_2H_4)$_2$ (**4**·C_2H_4) and (di)Pd($C_2H_3NO_2$)$_2$ (**5**·$C_2H_4NO_2$).

Pd(olefin)$_2$ complexes, **4**·C_2H_4 and **5**·$C_2H_4NO_2$, yields stable structures (the structures optimize to a local energy minimum and possess no imaginary frequency modes). In both complexes, the two olefins are oriented out of the N_2Pd plane, antiparallel with respect to each other (Figure 12). Several stereoisomers of the dinitroethylene complex, **5**·$C_2H_4NO_2$, are possible with different relative orientations of the two $-NO_2$ substituents (Figure S5). The lowest energy structure orients the nitro substituents in opposite directions (Figure 12), minimizing the molecular dipole.

The elongated C−C bonds of the coordinated olefins in **4**·C_2H_4 and **5**·$C_2H_4NO_2$, 1.40 and 1.42 Å, respectively, are slightly shorter than those in the corresponding monoolefin complexes, **4** and **5** (by 0.03 and 0.02 Å, respectively). This property probably reflects the need to distribute the back-bonding electron density on palladium between two olefin ligands.

The tetrahedral geometry common among L_4M^0 complexes of the group 10 metals[23] is not evident in **4**·C_2H_4 and **5**·$C_2H_4NO_2$. These structures are better described as pseudo-octahedral complexes. According to this description, **4**·C_2H_4 and **5**·$C_2H_4NO_2$ formally represent $L_2Pd^{IV}R_4$ complexes with metallacyclopropane-like metal−olefin interactions. The pseudoaxial Pd−C bonds are substantially longer (2.32 Å in both complexes) than the corresponding pseudoequatorial Pd−C bonds (**4**·C_2H_4, 2.23 Å; **5**·$C_2H_4NO_2$, 2.15 Å) (Table S4). The calculations reveal that coordination of the second olefin to **4** and **5** is energetically unfavorable with respect to the separated reagents: $\Delta G^\circ = 11.2$ and 8.1 kcal/mol, respectively, in CH_2Cl_2 (eqs 13 and 14).[24]

(22) For previous theoretical studies of d^{10} transition-metal−alkene complexes, see: (a) Ziegler, T.; Rauk, A. *Inorg. Chem.* **1979**, *18*, 1558−1565. (b) Kitaura, K.; Sakaki, S.; Morokuma, K. *Inorg. Chem.* **1981**, *20*, 2292−2297. (c) Ziegler, T. *Inorg. Chem.* **1985**, *24*, 1547−1552. (d) Morokuma, K.; Borden, W. T. *J. Am. Chem. Soc.* **1991**, *113*, 1912−1914. (e) Li, J.; Schreckenbach, G.; Ziegler, T. *Inorg. Chem.* **1995**, *34*, 3245−3252. (f) Uddin, J.; Dapprich, S.; Frenking, G.; Yates, B. F. *Organometallics* **1999**, *18*, 457−465.

(23) (a) Cotton, F. A.; Wilkinson, G.; Murillo, C. A.; Bochmann, M. *Advanced Inorganic Chemistry*, 6th ed.; Wiley: New York, 1999; p 1064. (b) The prototypical tetracoordinate L_4M complex, $Pd(PPh_3)_4$, exhibits a tetrahedral coordination environment: Andrianov, V. G.; Akhrem, I. S.; Chistovalova, N. M.; Struchkov, Y. T. *J. Struct. Chem.* **1976**, *17*, 111−116.

(24) The solvent is modeled computationally using the dipole polarizable continuum model (DPCM): (a) Miertuš, S.; Scrocco, E.; Tomasi, J. *Chem. Phys.* **1981**, *55*, 117−129. (b) Miertuš, S.; Tomasi, J. *Chem. Phys.* **1982**, *65*, 239−245. (c) Cossi, M.; Barone, V.; Cammi, R.; Tomasi, J. *Chem. Phys. Lett.* **1996**, *255*, 327−335.

This result rationalizes the inability to detect such species experimentally.

$$\underset{\mathbf{4}}{\text{(di)Pd}(C_2H_4)} + C_2H_4 \underset{CH_2Cl_2}{\overset{\Delta G_{calc} = 11.2\ \text{kcal/mol}}{\rightleftharpoons}} \underset{\mathbf{4}\cdot C_2H_4}{\text{(di)Pd}(C_2H_4)_2} \quad (13)$$

$$\underset{\mathbf{5}}{\text{(di)Pd}(C_2H_3NO_2)} + C_2H_3NO_2 \underset{CH_2Cl_2}{\overset{\Delta G_{calc} = 8.1\ \text{kcal/mol}}{\rightleftharpoons}} \underset{\mathbf{5}\cdot C_2H_3NO_2}{\text{(di)Pd}(C_2H_3NO_2)_2} \quad (14)$$

Transition-state structures, **[4**/C_2H_4**]**‡ and **[5**/$C_2H_4NO_2$**]**‡, were identified and optimized for these reactions (Figure 13, Tables S4 and S5). In **[4**/C_2H_4**]**‡, the incoming ethylene interacts with palladium along the axial direction, with one of the two approaching carbon atoms interacting slightly more strongly with the palladium center: $d_{Pd-C(axial)} = 2.91$ Å and $d_{Pd-C(equatorial)} = 3.08$ Å. The two carbon atoms of the pre-existing ethylene ligand have slipped from the equatorial plane toward the pseudo-octahedral sites they occupy in the intermediate, **4**·C_2H_4. In the nitroethylene transition state, **[5**/$C_2H_4NO_2$**]**‡, the β-carbon of nitroethylene occupies a pseudo-axial coordination site, and in contrast to the ethylene transition state, the α-carbon and nitro group lie in the direction of the diimine ligand (Figure 13). The β-carbon is more closely associated with palladium than the α-carbon: $d_{Pd-C\alpha} = 2.31$ Å and $d_{Pd-C\beta} = 2.60$ Å.

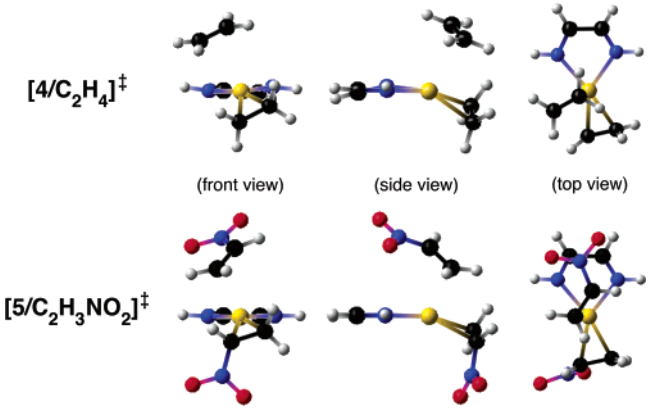

Figure 13. Ball-and-stick models of the minimized transition structures, **[4**/C_2H_4**]**‡ and **[5**/$C_2H_4NO_2$**]**‡.

Free energies of the transition states were calculated relative to the separated reagents in CH_2Cl_2 (**[4**/C_2H_4**]**‡, 16.3 kcal/mol; **[5**/$C_2H_4NO_2$**]**‡, 13.2 kcal/mol at 298 K). Perhaps fortuitously, these activation energies are remarkably similar to those obtained from the experimental studies of β-nitrostyrene self-exchange reactions in CH_2Cl_2 (14.4−17.7 kcal/mol at 298 K, Table 2), and the electron-deficient alkene, nitrostyrene, experiences a lower barrier than ethylene (cf. Figure 5).

Computational Analysis of Solvent Effects. The calculations reveal moderate solvent effects on the reaction. The relative free energies of all structures in the ethylene and nitroethylene-substitution reactions increase when toluene is modeled as the solvent rather than dichloromethane.[24] In both reactions, the solvent effect is more pronounced in the ground state than in the transition state (Figure 14), and therefore, the reactions encounter a lower energy barrier ($\Delta G^{\ddagger}$) in toluene. This result

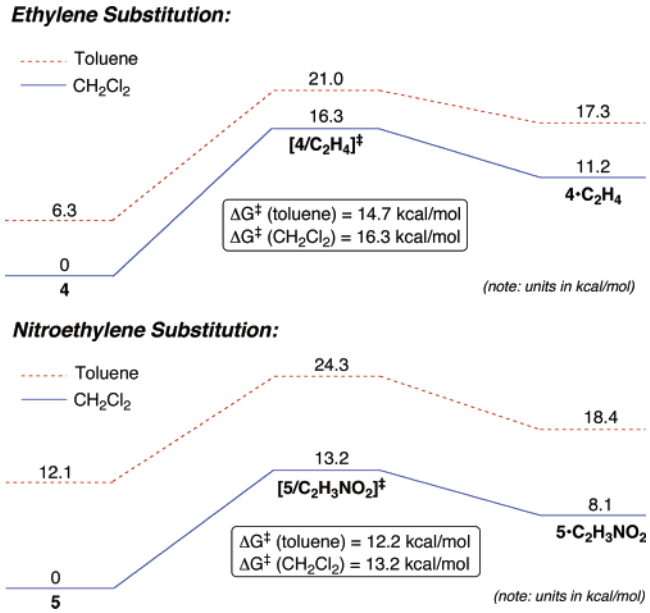

Figure 14. Influence of solvent on the olefin-substitution reactions.

Table 3. Calculated Dipole Moments of the Optimized Structures in Dichloromethane and Toluene

structure	$\mu_{CH_2Cl_2}$ (D)	$\mu_{toluene}$ (D)
4	7.3	6.6
C_2H_4	0	0
[**4**/C_2H_4]‡	5.3	4.8
5	13.8	12.4
$C_2H_3NO_2$	5.3	5.0
[**5**/$C_2H_3NO_2$]‡	5.2	5.4

agrees qualitatively with the experimental data, which reveal higher reaction rates in toluene than in dicholoromethane (Figure 9).

The solvent effect can be rationalized by considering the relative stabilization of more polar molecules in polar solvents. Dipole moments of the reagents and transition states in these reactions have been calculated (Table 3), and indeed, the palladium(0)−olefin adducts, **4** and **5**, are more polar than those of the transition states, **[4**/C_2H_4**]**‡ and **[5**/$C_2H_3NO_2$**]**‡.

Analysis of Orbital Interactions in Olefin-Substitution Reactions. Intrinsic reaction coordinate (IRC) calculations[25] were conducted for both ligand-substitution reactions by starting with the gas-phase transition-state structures, **[4**/C_2H_4**]**‡ and **[5**/$C_2H_3NO_2$**]**‡, and following the low-energy pathways backward toward the separated reagents, **4** + C_2H_4 and **5** + $C_2H_3NO_2$, and forward to the diolefin intermediates, **4**·C_2H_4 and **5**·$C_2H_3NO_2$. Several structures along the reaction coordinate were selected for analysis by natural bond orbital (NBO) methods[26] in order to identify the principal orbital interactions that take place between palladium and the incoming olefin (Schemes 2 and 3).

In both ligand-substitution reactions (**4** + C_2H_4; **5** + $C_2H_3NO_2$), the incoming olefin approaches the palladium center with

(25) The intrinsic reaction coordinate (IRC) is defined by the single imaginary frequency of the optimized transition state. This frequency defines the landscape in which reactants approach the transition state and the transition state proceeds to the product. The IRC algorithm iteratively steps down the reaction surface until the reactant and product ground-state geometries are found. (a) Gonzalez, C.; Schlegel, H. B. *J. Chem. Phys.* **1989**, *90*, 2154−2161. (b) Gonzalez, C.; Schlegel, H. B. *J. Phys. Chem.* **1990**, *94*, 5523−5527.

Scheme 2. Natural Bond Orbital Plots Depicting the Principal Orbital Interactions That Occur along the Reaction Coordinate for Ethylene Substitution in **4**

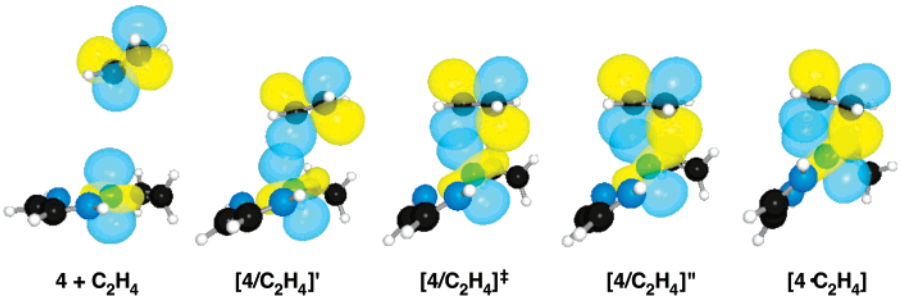

Scheme 3. Natural Bond Orbital Plots Depicting the Principal Orbital Interactions That Occur along the Reaction Coordinate for Nitroethylene Substitution in **5**

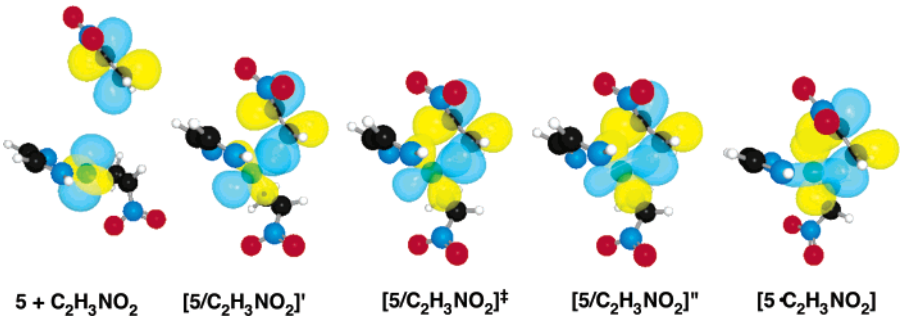

an approximately 110° angle between the face of the olefin and the trigonal plane of the palladium complex (Schemes 2 and 3). Analysis of the orbital interactions at an early stage in the reaction (structures **[4**/C_2H_4]′ and **[5**/$C_2H_3NO_2$]′) reveals the development of significant overlap between a palladium-centered lone pair in an orbital of $\sim d_{x^2-y^2}$ character[27] and the empty π^* orbital of the olefin. This angle of attack, ∠Pd−C−C ≈ 105−110°, resembles the Bürgi−Dunitz trajectory[28] associated with nucleophilic attack at the π^* orbital of carbonyl groups in organic chemistry (Figure 15). Rehybridization of the palladium-based orbital as the olefin continues along the reaction coordinate enables more extensive Pd → olefin π-back-bonding in the diolefin intermediates.[16]

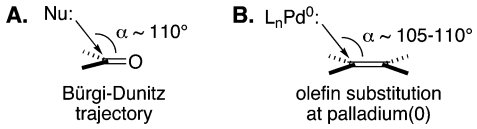

Figure 15. Relationship between the trajectory of attack at sp^2-hybridized carbon centers in (A) the addition of nucleophiles to carbonyl groups and (B) olefin substitution at palladium(0).

Natural charges[29] were calculated for each of the structures identified in Schemes 2 and 3, and this analysis (Tables 4 and 5) reveals the direction of charge transfer along the reaction coordinate Pd → olefin. The incoming olefins acquire a partial negative charge, with the corresponding positive charge accumulated on the palladium fragment.

Table 4. NBO-Derived Natural Charges for the Palladium Fragment, **4**, and Ethylene along the Reaction Coordinate for Ethylene Exchange (See Scheme 2)

fragment	**4** + C_2H_4[a]	[**4**/C_2H_4]′	[**4**/C_2H_4]‡	[**4**/C_2H_4]″	**4**·C_2H_4
4	<0.001	0.008	0.013	0.141	0.155
C_2H_4	< −0.001	−0.008	−0.013	−0.141	−0.155

[a] The palladium center and nearest carbon atom of ethylene were fixed at a distance of 5 Å.

Table 5. NBO-Derived Natural Charges for the Palladium Fragment, **5**, and Nitroethylene along the Reaction Coordinate for Nitroethylene Exchange (See Scheme 3)

fragment	**5** + $C_2H_3NO_2$[a]	[**5**/$C_2H_3NO_2$]′	[**5**/$C_2H_3NO_2$]‡	[**5**/$C_2H_3NO_2$]″	**5**·$C_2H_3NO_2$
5	0.002	0.191	0.277	0.342	0.401
$C_2H_3NO_2$	−0.002	−0.191	−0.277	−0.342	−0.401

[a] The palladium center and nearest carbon atom of nitroethylene were fixed at a distance of 5 Å.

Inverse-Electron-Demand Ligand-Substitution Reactions: Comparison with Traditional Ligand Substitution. The olefin exchange reactions described above challenge several traditional concepts in ligand-substitution chemistry. The trigonal palladium−olefin complexes, $\mathbf{3^X}$, possess 16 valence electrons, and such complexes are said to undergo ligand substitution by an *associative* mechanism because they are "coordinatively unsaturated".[30] This description is built on the assumption that complexes with fewer than 18 valence electrons possess a vacant metal-based orbital to interact with the incoming ligand. The concept of coordinative saturation/unsaturation, however, loses significance for palladium(0) and related d^{10} metal complexes (e.g., nickel(0) and copper(I)), which lack such a low-energy

(26) (a) Glendening, E. D.; Badenhoop, J. K.; Reed, A. E.; Carpenter, J. E.; Bohmann, J. A.; Morales, C. M.; Weinhold, F. *NBO 5.0*; Theoretical Chemistry Institute, University of Wisconsin, Madison, 2001. (b) Foster, J. P.; Weinhold, F. *J. Am. Chem. Soc.* **1980**, *102*, 7211−7218. (c) For a general review, see: Weinhold, F. In *Encyclopedia of Computational Chemistry*; Schleyer, P. v. R., Allinger, N. L., Clark, T., Gasteiger, J., Kollman, P. A., Schaefer, H. F., III, Schreiner, P. R., Eds.; Wiley: Chichester, 1998; Vol. 3, pp 1792−1811.

(27) The coordinate system is defined by the orientation of the d_{z^2}-shaped orbital identified by the DFT calculations. This orbital in the trigonal palladium olefin complexes, **4** and **5**, lies in the molecular plane parallel to the coordinated olefin. According to this orientation, the orbital in the axial direction is the $d_{x^2-y^2}$ orbital.

(28) Bürgi, H. B.; Dunitz, J. D.; Lehn, J. M.; Wipff, G. *Tetrahedron* **1974**, *30*, 1563−1572.

(29) Reed, A. E.; Weinstock, R. B.; Weinhold, F. *J. Chem. Phys.* **1985**, *83*, 735−746.

(30) Reference 8b, p 236.

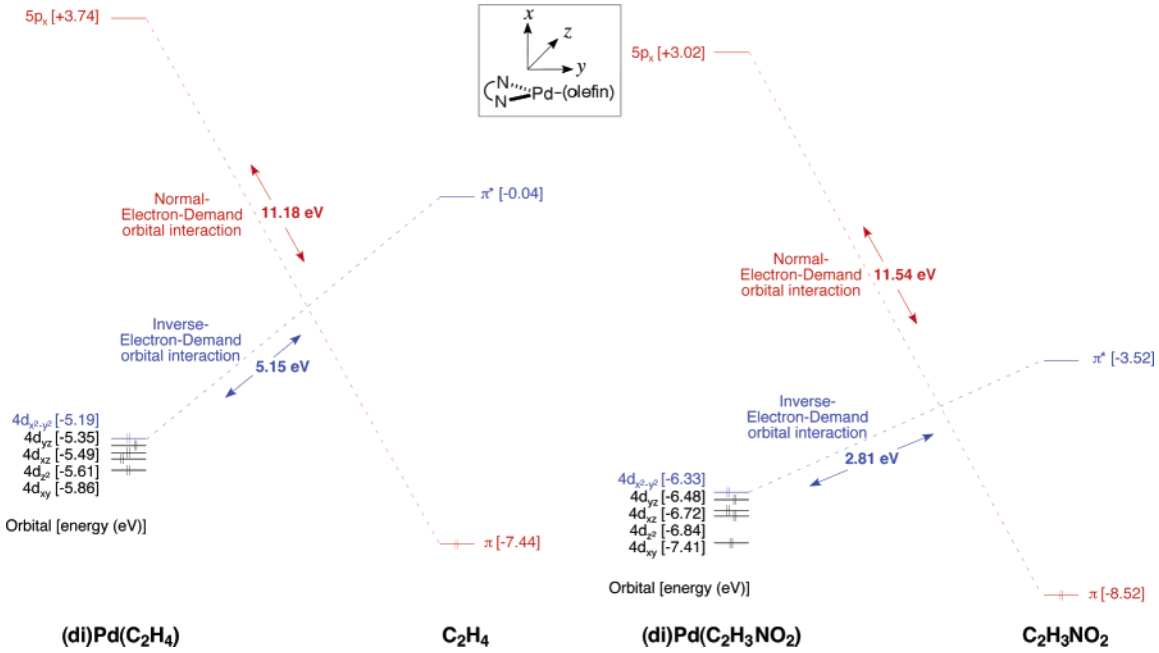

Figure 16. Calculated energies of the frontier Kohn−Sham orbitals for isolated (di)Pd(C_2H_4) (**4**), C_2H_4, (di)Pd($C_2H_3NO_2$) (**5**), and $C_2H_3NO_2$. The inverse-electron-demand character of olefin substitution at palladium(0) originates from the better energy match between the Pd-4d and olefin-π* orbitals relative to the olefin-π and Pd-acceptor orbitals.

orbital (see below). For example, even highly unsaturated, 12-electron monophosphine−palladium(0) complexes react as electron-rich species, undergoing efficient oxidative addition of aryl halides.[31]

In traditional ligand-substitution reactions, the principal orbital interaction involves the HOMO on the ligand and LUMO on the metal (Figure 1). In the present system, however, the principal interaction occurs between the HOMO on palladium and the LUMO of the alkene (Schemes 2 and 3). The Kohn−Sham orbital energies calculated for the reaction partners **4**/C_2H_4 and **5**/$C_2H_3NO_2$ illustrate this point (Figure 16). The Pd-4d and olefin-π* orbitals are significantly better matched energetically than the corresponding olefin-π and Pd-acceptor orbitals. The most reasonable acceptor orbital on palladium is a p_x-orbital, with an energy of +3.74 and +3.02 eV for **4** and **5**, respectively. In accordance with qualitative perturbation molecular orbital (PMO) analysis, the smaller donor−acceptor energy gap betweeen the Pd-4d and olefin-π* orbitals relative to the olefin-π and Pd-acceptor orbitals correlates with greater stabilization at the transition state. This qualitative PMO analysis is clearly opposite to that of traditional ligand-substitution reactions (Figure 1).

On the basis of this analysis, olefin exchange at palladium(0) may be defined as an "inverse-electron-demand" ligand-substitution reaction.[32] This reaction class was considered in a prominent textbook, but it was dismissed: ligand-substitution reactions are "well known for M_E + N (metal electrophile plus reagent nucleophile), but the two-electron pathway with M_N + E leads either to a Lewis acid−base adduct (M_N−E) or to oxidative-addition rather than to a substitution reaction."[33] Despite this statement, earlier studies had provided indirect[34] and direct[35] experimental support for the principle of inverse-electron-demand ligand substitution, and the systematic experimental and computational results of the present study provide a clear exception to this observation.

Nevertheless, the textbook statement highlights the relationship between inverse-electron-demand ligand-substitution reactions and other well-established modes of nucleophilic transition-metal reactivity.[36] Olefin substitution at palladium(0) is a redox-neutral process, yet the reaction trajectory closely resembles that of heterolytic oxidative addition reactions. The oxidative addition of methyl iodide to iridium(I) of Vaska's complex occurs via nucleophilic attack by an iridium lone-pair at the σ* orbital of methyl iodide (eq 15).[37] Wayland and co-workers have proposed that anionic rhodium(I)−porphyrin complexes exhibit similar nucleophilic reactivity in the activation of carbon monoxide and other electrophiles.[38,39] Consistent with this description, Goldman and Krogh-Jespersen studied the addition of carbon monoxide to Vaska's complex by computational methods and identified a bent transition state. This geometry reflects nucleophilic attack by iridium(I) at the π* orbital of CO (eq 16).[39]

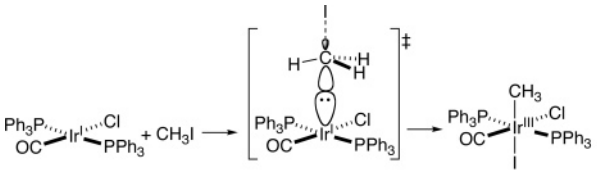

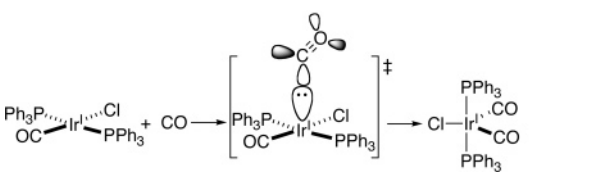

(31) (a) Littke, A. F.; Fu, G. C. *Angew. Chem., Int. Ed.* **2002**, *41*, 4176−4211. (b) Stambuli, J. P.; Bühl, M.; Hartwig, J. F. *J. Am. Chem. Soc.* **2002**, *124*, 9346−9347.
(32) This nomenclature is borrowed from the description of pericyclic reactions in organic chemistry. (a) Fleming, I. *Frontier Orbitals and Organic Chemical Reactions*; Wiley: New York, 1976. (b) Carruthers, W. *Cycloaddition Reactions in Organic Synthesis*; Pergamon Press: New York, 1990.
(33) Reference 8b, p 238.

Implications and Conclusion

With the growing use of electron-rich, d^{10} transition metals in catalysis, principles derived from the present study are likely to have broad application. Nickel(0) complexes, for example, have proven to be effective catalysts for the reductive coupling of unsaturated substrates, including alkenes, alkynes, and CO_2.[2] A recent study of the addition of CO_2 to a nickel(0)−diene complex revealed an associative mechanism.[40] According to the principles outlined above, this "association" probably involves nucleophilic attack of the electron-rich nickel(0) complex on the electrophilic CO_2 molecule. Organocuprate additions to α,β-unsaturated ketones also proceed by an associative mechanism, and recent computational studies highlight the nucleophilic reactivity of the electron-rich copper(I) center with the electron-deficient alkene.[3b] This interaction is sufficiently strong that the adduct is commonly drawn as a copper(III) complex, thereby blurring the distinction between ligand association and oxidative addition (eq 17).

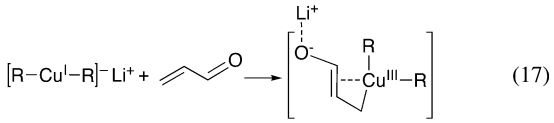

(17)

The present study was initiated following our observation that oxygenation of palladium(0) (eq 7) appears to proceed by a mechanism resembling ligand substitution. Upon completion of this study of ligand substitution at palladium(0), however, we suggest that the converse relationship is perhaps more appropriate and meaningful: ligand substitution at palladium(0) proceeds by a mechanism resembling oxidative addition. Ongoing studies in our laboratory continue to probe the relationship between alkene and dioxygen reactivity, particularly to identify the impact of the substrate electronic properties (i.e., triplet versus singlet) on the reaction mechanism (eqs 7 and 8).

Experimental Section

General Considerations. All syntheses and subsequent handling of palladium complexes were performed under a nitrogen atmosphere using either a glovebox (MBraun) or standard Schlenk techniques. Dichloromethane (Fisher) was purified by passing it over a column of activated alumina (A-2, Purifry), and toluene (Aldrich), hexanes (Aldrich), and diethyl ether (Aldrich) were purified by passing them over a column of activated alumina (A-2, Purifry) and a column of Q-5 oxygen scavenger (Engelhard). Dichloromethane-d_2 and toluene-d_8 were obtained from Cambridge Isotope Laboratories, Inc. and were dried for 24 h over CaH_2 and Na^0/benzophenone, respectively. Deuterated solvents were thoroughly degassed and stored in the glovebox. (bc)Pd(dba), **1**,[6a] and the (bc)Pd(ns^X) derivatives, $\mathbf{3^X}$,[10] were synthesized according to previously published methods. All β-nitrostyrene derivatives were obtained from Aldrich or Fluka and were used as received. NMR spectroscopic data were obtained at 27.0 °C, unless otherwise noted, using a Varian Unity 500 MHz, a Varian Inova 500 MHz, a Bruker Avance 360 MHz, or a Bruker AC 300 MHz spectrometer.

Characterization of (bc)Pd(ns^X) Derivatives, $\mathbf{3^X}$. In addition to the previously reported characterization data for the $\mathbf{3^X}$ derivatives (^{1}H and ^{13}C NMR spectroscopy, X-ray),[10] we have used indirect multinuclear correlation NMR spectroscopic methods (gHSQC[41] and gHMBC[42]) in order to assign the identity of the two coordinated olefin resonances. From these studies, the upfield resonance of the coordinated olefin corresponds to the proton adjacent to the phenyl ring and the downfield resonance corresponds to the proton adjacent to the nitro group (for details, see Figures S1 and S2, Tables S1 and S2).

Temperature-Dependent Equilibrium Studies. All data were acquired using a Bruker Avance 360 MHz spectrometer. Experimental samples were prepared in the glovebox and sealed under a nitrogen atmosphere, and upon removal from the glovebox, they were maintained at −78 °C until data collection was initiated. The temperature of the NMR probe was calibrated using a 99.7% CH_3OH/0.3% HCl standard sample,[43] and spectra were obtained after the sample had equilibrated at the set temperature for at least 25 min. The equilibrium constants at varying temperatures were derived from the integrations of the bound olefin resonances. Absolute concentrations of (bc)Pd($ns^{X/X'}$) and $ns^{X'/X}$ species were obtained by using 1,3,5-tri-*tert*-butylbenzene as an internal standard.

Temperature-Dependent Olefin-Exchange Kinetics Based on ^{1}H NMR Line Width Measurements. All data were acquired on a Varian Unity 500 MHz spectrometer. Sample preparation and temperature calibration were performed in the manner described above. GNMR v4.1 was used to simulate the line shape for the methine resonances of the bound olefin. The simulations were compared with the experimental spectra to calculate the line width at half-height.

UV−Visible Kinetic Studies. All UV−visible kinetics data were acquired on a pc-controlled Cary 3E spectrophotometer using WinUV 2.01 software. A Cary 1×1 peltier temperature controller was used to regulate the sample temperature at 25 °C. Solutions of known concentration were used to determine extinction coefficients for the reactants and products by the method of Beer's law. A representative experiment for the cross-exchange reaction between different olefins follows. Stock solutions of (bc)Pd(ns^{CH_3}) (1 mM) and ns^{CF_3} (2mM) in dichloromethane were prepared in the glovebox and removed from the glovebox in a Schlenk tube equipped with a 4 mm Kontes Teflon valve. The (bc)Pd(ns^{CH_3}) stock solution was maintained at −78 °C to avoid decomposition of the palladium complex. A gas-tight UV−visible cell equipped with a side-arm reservoir was used to allow both stock solutions to be added to the cell under a nitrogen atmosphere prior to initiating the reaction. The palladium stock solution (300μL) and dichloromethane (2.55 mL) were added via gas-tight syringe to the UV−visible cell, and the ns^{CF_3} solution (150 μL) was added to the side-arm. After the initial absorbance reading of the (bc)Pd(ns^{CH_3}) solution was obtained, the contents of the cell and side-arm were mixed rapidly, and single-wavelength (425 nm) data collection was initiated. Most reactions were complete (>5 half-lives) within ∼5 min. A text file of the data was imported into Microsoft Excel for data fitting. A kinetic model based on the bimolecular approach to equilibrium was employed, and the data were fit by minimizing the sum of the squared deviations between the experimental data and a fourth-order Runge−Kutta numerical simulation of the kinetic model. The equilibrium constants for olefin binding were required for fitting and were obtained by ^{1}H NMR spectroscopic experiments, as described above.

A representative experiment for the olefin cross-exchange reaction with varying solvent dielectric follows. Stock solutions of (bc)Pd(ns^{CH_3})

(34) (a) Pearson, R. G.; Gray, H. B.; Basolo, F. *J. Am. Chem. Soc.* **1960**, *82*, 787−792. (b) Gray, H. B. *J. Am. Chem. Soc.* **1962**, *84*, 1548−1552. (c) Belluco, U.; Cattalini, L.; Turco, A. *J. Am. Chem. Soc.* **1964**, *86*, 226−229. (d) Cattalini, L.; Orio, A.; Nicolini, M. *J. Am. Chem. Soc.* **1966**, *88*, 5734−5738.
(35) van Gaal, H. L. M.; van der Ent, A. *Inorg. Chim. Acta* **1973**, *7*, 653−659.
(36) Henderson, S.; Henderson, R. A. *Adv. Phys. Org. Chem.* **1987**, *23*, 1−62.
(37) (a) Chock, P. B.; Halpern, J. *J. Am. Chem. Soc.* **1966**, *88*, 3511−3514. (b) Burgess, J.; Hacker, M. J.; Kemmitt, R. D. W. *J. Organomet. Chem.* **1974**, *72*, 121−126.
(38) (a) Wayland, B. B.; Balkus, K. J., Jr.; Farnos, M. D. *Organometallics* **1989**, *8*, 950−955. (b) Fu, X.; Basickes, L.; Wayland, B. B. *Chem. Commun.* **2003**, 520−521.
(39) Abu-Hasanayn, F.; Krogh-Jespersen, K.; Goldman, A. S. *J. Am. Chem. Soc.* **1994**, *116*, 5979−5980.
(40) Geyer, C.; Schindler, S. *Organometallics* **1998**, *17*, 4400−4405.
(41) Bodenhausen, G.; Ruben, D. J. *Chem. Phys. Lett.* **1980**, *69*, 185−189.
(42) Bax, A.; Summers, M. F. *J. Am. Chem. Soc.* **1986**, *108*, 2093−2094.
(43) Van Geet, A. L. *Anal. Chem.* **1970**, *42*, 679−680.

(2.4 mM) and ns^{OCH_3} (24.2 mM) in dichloromethane were prepared as described above. Into a UV−visible cell were added (bc)Pd(ns^{CH_3}) (150 μL) and a ratio of dichloromethane/toluene (2.6 mL total volume), and ns^{OCH_3} (250 μL) was added to the side-arm. The mole fraction of dichloromethane/toluene was varied (1.00, 0.83, 0.67, 0.50, 0.37, 0.17, and 0.07) while the [Pd], [ns^{OCH_3}], and total reaction volume were held constant. Data at the solvent mole fraction of 0.07 were obtained by similar methods, with the exception that toluene was used to prepare the stock solutions. The reaction was monitored at a single wavelength (445 nm) over 4 min, although most reactions were complete (>5 half-lives) after ~90 s. Each reaction, at varying solvent ratios, was performed in triplicate, and the entire sequence of reactions was duplicated. A text file of the reaction time-course was imported into Microsoft Excel for fitting. The pseudo-first-order integrated rate law was used to fit the data. A zero-order decomposition term was also required in the rate expression to achieve an adequate fit of the data (eq 18). Four parameters (k_{obs}, m, A_0, A_{inf}) were varied in order to minimize the sum of the squared deviations between the experimental data and the nonlinear least-squares fit. A representative data set and fit is shown in Figure 8A.

$$A_t = (A_\infty + (A_0 - A_\infty)\exp(-k_{obs}t)) + mt \qquad (18)$$

Computational Methods. The Gaussian 98 program suite[44] was used to carry out all calculations. The combined Becke three-parameter hybrid exchange functional (Becke3)[45a] with the Lee−Yang−Parr correlation functional (LYP),[46] known as B3LYP,[45b] was employed for all calculations using DFT methods.[47] All ground-state structures in the gas phase were optimized using the two-shell double-ζ basis set developed by Hay and Wadt (LANL2DZ) combined with a relativistic effective core potential (RECP).[48] The Dunning−Huzinaga double-ζ basis set (D95) was used on all H and second-row elements.[49] Structures were verified as local minima by frequency analysis. The gas-phase transition-state structures were optimized using the QST3[50] option available within Gaussian 98. Subsequent analytical frequency calculations were performed to verify that the saddle point corresponded to exactly one imaginary frequency. Using the calculated force constant matrix from the frequency analysis of the optimized transition structure, the intrinsic reaction coordinate (IRC)[25] in the gas phase was followed in both directions from the transition states to define the reaction trajectory. Population analysis along the reaction trajectory was performed using the NBO 5.0[26] program available within Gaussian 98, and NBOView[26] was used for orbital visualizations. Solvation effects were determined at two dielectric constants (2.379 for toluene and 8.93 for dichloromethane) using the dipole polarizable continuum model (DPCM)[24] for optimization of all ground-state and transition-state structures at the RB3LYP/LANL2DZ level. Only the dielectric constant was specified in the above solvation calculations; all other parameters defining the solvent were left as the Gaussian 98 default values. Geometry optimizations were also performed with a higher level basis set, Stuttgart RSC 1997 ECP for Pd[51] and 6-311++G** for C, N, and H,[52] for the degenerate exchange of ethylene on (diimine)Pd(ethylene) both in the gas phase and in the above solvent models. Analysis of the basis-set effects on the results are provided in the Supporting Information.

Acknowledgment. This work was supported by the Dreyfus Foundation (New Faculty and Teacher-Scholar Award), the Sloan Foundation (Research Fellowship), and the NSF (CAREER Award, CHE-0094344). Funding for NMR instrumentation is provided by NIH (1 S10 RR04981-01 and 1 S10 RR08389-01) and the NSF (CHE-8813550, CHE-9629688, CHE-9629688, CHE-9208463, and CHE-9709065).

Supporting Information Available: 2D NMR spectroscopic data of $\mathbf{3}^{CH_3}$, additional kinetics data, comparison of X-ray and computational structural parameters, basis-set comparisons, and computational output files. This material is available free of charge via the Internet at http://pubs.acs.org.

JA0459734

(44) Frisch, M. J.; Trucks, G. W.; Schlegel, H. B.; Scuseria, G. E.; Robb, M. A.; Cheeseman, J. R.; Zakrzewski, V. G.; Montgomery, J. A., Jr.; Stratmann, R. E.; Burant, J. C.; Dapprich, S.; Millam, J. M.; Daniels, A. D.; Kudin, K. N.; Strain, M. C.; Farkas, O.; Tomasi, J.; Barone, V.; Cossi, M.; Cammi, R.; Mennucci, B.; Pomelli, C.; Adamo, C.; Clifford, S.; Ochterski, J.; Petersson, G. A.; Ayala, P. Y.; Cui, Q.; Morokuma, K.; Malick, D. K.; Rabuck, A. D.; Raghavachari, K.; Foresman, J. B.; Cioslowski, J.; Ortiz, J. V.; Baboul, A. G.; Stefanov, B. B.; Liu, G.; Liashenko, A.; Piskorz, P.; Komaromi, I.; Gomperts, R.; Martin, R. L.; Fox, D. J.; Keith, T.; Al-Laham, M. A.; Peng, C. Y.; Nanayakkara, A.; Challacombe, M.; Gill, P. M. W.; Johnson, B.; Chen, W.; Wong, M. W.; Andres, J. L.; Gonzalez, C.; Head-Gordon, M.; Replogle, E. S.; Pople, J. A. *Gaussian 98*, Revision A.9; Gaussian, Inc.: Pittsburgh, PA, 1998.
(45) (a) Becke, A. D. *J. Chem. Phys.* **1993**, *98*, 1372−1377. (b) Becke, A. D. *J. Chem. Phys.* **1993**, *98*, 5648−5652.
(46) Lee, C.; Yang, W.; Parr, R. G. *Phys. Rev. B* **1988**, *37*, 785−789.
(47) For general references on DFT methods, see: Koch, W.; Holthausen, M. C. *A Chemist's Guide to Density Functional Theory*, 2nd ed.; Wiley-VCH: Weinheim, 2001.
(48) (a) Hay, P. J.; Wadt, W. R. *J. Chem. Phys.* **1985**, *82*, 270−283. (b) Wadt, W. R.; Hay, P. J. *J. Chem. Phys.* **1985**, *82*, 284−298. (c) Hay, P. J.; Wadt, W. R. *J. Chem. Phys.* **1985**, *82*, 299−310.
(49) Dunning, T. H., Jr.; Hay, P. J. In *Modern Theoretical Chemistry*; Schaefer, H. F., III, Ed.; Plenum Press: New York, 1977.
(50) (a) Peng, C.; Schlegel, H. B. *Isr. J. Chem.* **1993**, *33*, 449−454. (b) Peng, C.; Ayala, P. Y.; Schlegel, H. B.; Frisch, M. J. *J. Comput. Chem.* **1996**, *17*, 49−56.
(51) (a) Bergner, A.; Dolg, M.; Küchle, W.; Stoll, H.; Preuss, H. *Mol. Phys.* **1993**, *80*, 1431−1441. (b) Kaupp, M.; Schleyer, P. v. R.; Stoll, H.; Preuss, H. *J. Chem. Phys.* **1991**, *94*, 1360−1366. (c) Dolg, M.; Wedig, U.; Stoll, H.; Preuss, H. *J. Chem. Phys.* **1987**, *86*, 866−872. (d) Dolg, M.; Stoll, H.; Preuss, H.; Pitzer, R. M. *J. Phys. Chem.* **1993**, *97*, 5852−5859.
(52) Hehre, W. J.; Radom, L.; Schleyer, P. v. R.; Pople, J. A. *Ab Initio Molecular Orbital Theory*; Wiley: New York, 1986.